First passage times for nonlinear ship dynamics using Gaussian random fields and effective waves

Leo Dostal[a,], Marten Hollm[a], Atsuo Maki[b]

[a] *Institute of Mechanics and Ocean Engineering, Hamburg University of Technology, 21073 Hamburg, Germany*
[b] *Graduate School of Engineering, Osaka University, 2-1 Yamadaoka, Suita, Osaka, Japan*

Abstract

It is important to know the mean time until critical roll motion occurs in various operating and sea conditions, in order to determine and ensure the safety of ship designs and operating ships. Since typical ocean waves are irregular, the forcing and roll response of the ship is considered to be a stochastic process of colored noise type. However, the simulation of the corresponding first passage times is very time consuming. Therefore, an approach for the determination of mean first passage times of critical roll motion of ships is proposed in this paper which needs much less computation time. This approach is based on explicit formulas for the roll energy of the ship. These formulas are used to determine the mean first passage times based on integral expressions, which were previously obtained. The resulting integral expressions can be computed very fast using standard quadrature formulas. Moreover, the underlying model for ship dynamics is extended by introducing a new effective wave for short-crested sea states. This is an extension to the improved Grim's effective wave concept.

Keywords: effective wave, first passage times, irregular seas

1. Introduction

Large amplitude rolling is one of the dangerous dynamic responses of a ship traveling in ocean waves. A very dangerous case of large amplitude roll

motion of a ship is parametric rolling, which is the resonant case when waves encounter the ship approximately twice per roll period. In order to increase the safety of ocean going ships, it is important to know the mean time until critical roll motion occurs in a given sea state. This is necessary for ship design as well as for maneuvering decisions of ships in ocean waves. Typical ocean waves are irregular, therefore it is necessary to use probability theory in order to determine the desired mean first passage times. For this reason, the roll response of the ship is considered to be a stochastic process, which is of colored noise type, e.g. [1].

Concerning nonlinear ship roll dynamics in ocean waves, it is well known that the righting lever curve of a ship changes in waves as they pass the ship hull, leading to a considerable difference in wave trough conditions compared to wave crest conditions, e.g. [2, 3, 4, 5]. From this insight it is clear that it is a challenging problem to efficiently determine the instantaneous righting lever in irregular ocean waves. This problem has been considered by Grim, who developed a sinusoidal effective wave with variable amplitude based on the instantaneous wave surface [6]. Based on this work, Bulian developed an improved Grim's effective wave [7]. Moreover, the concept of Grim's effective wave for short crested irregular seas is stated by Umeda and Yamakoshi in [8]. Also, the Volterra series approach [9] can be used in order to address this problem. A comparison between Grim's effective wave, the improved Grim's effective wave and the Volterra series approach can be found in [10]

So far, a lot of approaches have been used for stochastic assessment of ship rolling. Blocki calculated the capsizing probability for the case of parametric rolling. In his method, the estimation was separated into a deterministic and a random process. Combining both results, the capsizing probability was calculated [11]. Following his methodology, Themelis and Spyrou proposed a stochastic assessment method of parametric rolling. In their paper, the occurrence probability of parametric rolling in irregular seas is assumed as the probability of encountering critical wave groups [12]. One of the authors also applied the wave group theory, whereby the corresponding results are combined with the deterministic results of parametric rolling in regular seas. With this, a probability index of parametric rolling is calculated[13]. In that paper the probability index of parametric rolling is defined as the ratio of the number of events in which a ship encounters a wave group triggering off parametric rolling to the number of events in which it encounters a wave. Since this is not the occurrence probability of parametric rolling, this probability index was introduced.

For the problem of ship roll motion, Roberts[14] applied the stochastic averaging method. In his methodology, the results from Stratonovich[15] and Khasminskii[16] are used. By this means, the probability density function of the roll amplitude can be calculated from the obtained first order Itô's equation. However, the preliminaries required to apply the stochastic averaging method are not met in [14]. This was later improved by Roberts in the publications [17, 18] using series expansions. On the other hand, Dostal et al. [5] proposed the energy-based stochastic averaging method, which extended the results of [19] from white noise to colored noise. No series expansions are needed in this approach and the full nonlinearity is considered.

Since ship roll dynamics is nonlinear and the forcing due to ocean waves is irregular, the computation of first passage times for large amplitude roll motion is challenging. In [20, 21] the first passage problem of ship roll is studied using asymptotic expansions of Pontryagin's partial differential equation [22, 23]. Solutions of this equation are difficult to obtain for diffusion processes with two or more dimensions. Recently, first passage times for ship roll motion are determined using the path integral approach [24].

The aim of this paper is to incorporate the combination of newly established results on the improved effective wave for short crested seas, new mean first passage time formulas and new stochastic averaging formulas in the early design process of ships.

In addition, it is shown for the first time that the proposed procedure is of two orders of magnitude faster than corresponding Monte Carlo simulation. This important fact enables the use of the procedure in the early design process.

The procedure in this paper is much more useful compared to our earlier results in [5], where the mean first passage time formula is limited to be used only for a very small initial roll energy and the irregular sea state is limited to long-crested seas. The used stochastic averaging formulas for ship roll motion are generalized as well, such that general nonlinearities in the corresponding equations of motion can be used. This is another extension of [5], where only a cubic nonlinearity is used for roll restoring. Moreover, no results on the comparison of the obtained first passage times with Monte Carlo simulations were obtained before, since the computational costs for this task are very high.

The new improved effective wave for short crested seas is proposed in Sec. 3, which is an improvement of the effective wave presented by Bulian

in [7]. Moreover, new first passage time formulas, which were recently derived in [23], are used for the determination of mean first passage time of roll motion of ships to reach critical roll angles in Sec. 6. This is important for the determination of dangerous ship roll dynamics in ocean waves. The remaining parts of the paper include the modeling of irregular seas in Sec. 2, nonlinear ship dynamics in Sec. 4 and new generalized energy-based stochastic averaging formulas in Sec. 5.

2. Ship in Irregular seas

The wave motion is described in the reference frame $G(X, Y, Z)$, which is fixed with its origin G amidships, whereby the X-axis coincides with the ship forward direction. The XY-plane corresponds to the calm water plane and the Z-axis points upwards.

The superposition of harmonic waves is a well-known probabilistic model for random seas. The amplitude of the individual waves at a certain frequency depends on the considered sea spectrum. Here, we use the Pierson–Moskowitz (PM) spectrum and the Joint North Sea Wave Project (JONSWAP) spectrum, which can be defined in terms of the significant wave height H_s and the modal frequency ω_m.

The direction of the individual waves in the above defined ship fixed reference frame $G(X, Y, Z)$ is described by the angle χ. For $\chi = 0$ the individual wave direction coincides with the X-axis. Using this angle, the propagation function $D(\chi)$ causes a scattering of the directions of progress of the harmonic waves. This allows short-crested random seas to be modeled. The spread function $D(\chi)$ has to be normalized in such a way that

$$\int_{-\pi}^{\pi} D(\chi)\,\mathrm{d}\chi = 1 \tag{1}$$

is fulfilled. One of the simplest used spread functions is the Cosine-squared distribution [25, 26]. An example of such a spread function with adjustable spreading width is given by

$$D(\chi) = \frac{2}{\chi_R}\cos^2\left(\frac{\pi}{\chi_R}\left(\chi - \chi_0\right)\right), \quad \text{with } |\chi - \chi_0| \leq \frac{\chi_R}{2}, \tag{2}$$

where the directions of propagation of the harmonic waves are distributed around the main direction of progress of the waves χ_0 by means of a quadratic

cosine function and the parameter χ_R is used to adjust the maximal spreading angle around the main direction χ_0. Alternative propagation functions are given among others in [27].

The same as for χ, also the main wave direction coincides with the X-axis for $\chi_0 = 0$. Since the X-axis points in the ship forward direction, the ship is in following seas for $\chi_0 = 0$ and in head seas for $\chi_0 = 180°$. With this, the Gaussian random field of the wave surface of an irregular sea can be written as

$$Z(X,Y,t) = \int_0^\infty \int_{-\pi}^{\pi} \cos\big(\omega_0\, t - \kappa(\omega_0)\,(X\cos(\chi) + Y\sin(\chi)) + \epsilon(\omega_0,\chi)\big)\sqrt{2\,S(\omega_0)\,D(\chi)\,\mathrm{d}\chi\,\mathrm{d}\omega_0}, \tag{3}$$

with the wave number $\kappa(\omega_0)$, frequencies ω_0, and the one-sided spectral density $S(\omega_0)$. A wave surface that is already irregular at the initial time is achieved if a random phase shift $\epsilon(\omega_0,\chi)$ of the wave components is carried out. This phase shift is evenly distributed in the interval $[0; 2\pi)$. The above integral is not a Riemann integral, but a summation rule over the frequencies ω_0 and angles χ. The wave surface described by $Z(X,Y,t)$ is a function of the coordinates X, Y and the time t. The resulting wave surface $Z(X,Y,t)$ modeled by equation (3) is an ergodic Gaussian process [28, 29]. In long-crested irregular seas, all superposed harmonic waves have the same direction of propagation χ_0. Then, Eq. (3) can be reduced to

$$Z_{\mathrm{L}}(X,Y,t) = \int_0^\infty \cos\big(\omega_0\, t - \kappa(\omega_0)\,(X\cos(\chi_0) + Y\sin(\chi_0)) + \epsilon(\omega_0)\big)\sqrt{2\,S(\omega_0)\,\mathrm{d}\omega_0}. \tag{4}$$

If the ship moves with velocity U and meets the waves at an angle χ_0 with respect to the ship's forward direction, then the wave encounter frequency ω is given by

$$\omega = \omega_0 - \kappa(\omega_0)\,U\cos\chi_0 \tag{5}$$

and the spectrum with respect to the encounter frequency is

$$S_e(\omega) = S(\omega_0)\left|\frac{\mathrm{d}\omega_0}{\mathrm{d}\omega}\right|. \tag{6}$$

In this case the encounter spectrum $S_e(\omega)$ is used in equation (3) instead of $S(\omega_0)$. In order to evaluate Eq. (6), ω_0 has to be expressed in terms of the encounter frequency ω by inverting Eq. (5).

In shallow water the wave number is $\kappa(\omega_0) = \omega_0/\sqrt{g\,d}$. This leads to

$$\left|\frac{\mathrm{d}\omega_0}{\mathrm{d}\omega}\right| = \left|\frac{1}{1 - \frac{U}{\sqrt{g\,d}}\cos\chi_0}\right|. \tag{7}$$

In deep water the wave number is given by $\kappa(\omega_0) = \omega_0^2/g$. This leads for $\frac{U\cos\chi_0}{g} < 0$ to the expression

$$\left|\frac{\mathrm{d}\omega_0}{\mathrm{d}\omega}\right| = \left|\frac{1}{\sqrt{1 - \frac{4\,U\,\omega\cos\chi_0}{g}}}\right|. \tag{8}$$

For the cases where $\frac{U\cos\chi_0}{g} > 0$, the values of ω_0 corresponding to a specific value of the encounter frequency are not unique. For more details on the determination of the encounter wave spectrum in deep water for these cases we refer to [30, 31, 32, 33].

3. Approximation of irregular seas by effective waves

The stochastic process $Z(X, Y, t)$ of wave elevation of the irregular seas, as defined in Eq. (3), leads to an irregular waterline contour along the hull of the ship. This results in random variations of the forces and moments acting on the ship. In order to circumvent the integration of the pressure field over the submerged hull surface for any possible wave flow around the hull, an effective wave is determined which has approximately the same effect on the righting lever arms of the ship as the irregular wave surface $Z(X, Y, t)$ defined in Eq. (3). This problem was first studied by Grim in [2]. The effective wave used by Grim is always located amidships and has only a variable amplitude. An extension of Grim's effective wave including a variable wave phase was done by Bulian in [7]. However, these results consider only long-crested sea states. Bulian's effective wave is extended in the following to consider also short-crested sea states.

The irregular wave surface $Z(X, Y, t)$ in the above defined ship fixed coordinate system $G(X, Y, Z)$ is approximated by the following effective wave surface (see Fig. 1)

$$\begin{aligned} Z_{\mathrm{eff}}(X, Y, t) &= \eta_c(t)\cos\left(\frac{2\,\pi}{L}\,X\right) + \eta_s(t)\sin\left(\frac{2\,\pi}{L}\,X\right) \\ &= \eta(t)\cos\left(\frac{2\,\pi}{L}\,X + \psi(t)\right), \end{aligned} \tag{9}$$

where L is the length of the effective wave (in its propagation direction defined by χ_0). For most ship hulls a wave with the length of the ship's length between perpendiculars L_{pp} divided by $\cos\chi_0$ causes the largest variation of the righting lever arm. Therefore, the effective wave length is chosen as $L = L_{\text{pp}}/\cos\chi_0$. The random processes $\eta_c(t)$, $\eta_s(t)$, $\eta(t)$ and $\psi(t)$ of Z_{eff} are related as follows:

$$\eta(t) = \sqrt{\eta_s(t)^2 + \eta_c(t)^2}, \qquad \psi(t) = \arctan\left(\frac{\eta_s(t)}{\eta_c(t)}\right), \tag{10}$$

$$\eta_s(t) = \eta(t)\sin(\psi(t)), \qquad \eta_c(t) = \eta(t)\cos(\psi(t)). \tag{11}$$

The effective wave has to optimally approximate the wave elevation in the

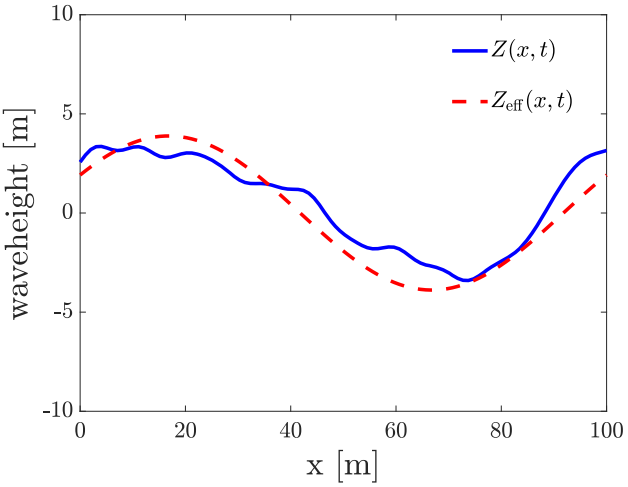

Figure 1: Irregular wave elevation Z (——) and effective wave Z_{eff} (- - -).

plain of main wave direction χ_0 at $Y = 0$ in the ship fixed coordinate system $G(X, Y, Z)$. The error between the wave surface $Z(X, 0, t)$ and the effective wave surface Z_{eff} is minimal if η_s and η_c are solutions of the following unconstrained quadratic optimization problem

$$\text{minimize} \quad I(\eta_s, \eta_c) = \int_{-L/2}^{L/2} \big(Z(X, 0, t) - Z_{\text{eff}}(X, Y, t)\big)^2 \mathrm{d}X. \tag{12}$$

The result for the short-crested sea state $Z(X, Y, t)$ is summarized in the following theorem.

Theorem 3.1. *The optimal solution of the optimization problem (12) is given by*

$$\eta_s(t) = \int_0^\infty f_s(\kappa(\omega)) \sin(\omega\, t + \epsilon(\omega)) \sqrt{2\, S(\omega)\, \mathrm{d}\omega}, \tag{13}$$

$$\eta_c(t) = \int_0^\infty f_c(\kappa(\omega)) \cos(\omega\, t + \epsilon(\omega)) \sqrt{2\, S(\omega)\, \mathrm{d}\omega}. \tag{14}$$

Here, the transfer functions f_s and f_c are given by

$$f_s(\kappa(\omega)) = \int_{-\pi}^{\pi} \frac{2\,\pi \sin r}{\pi^2 - r^2} \sqrt{D(\chi)\, \mathrm{d}\chi}, \qquad f_c(\kappa(\omega)) = \int_{-\pi}^{\pi} \frac{2\, r \sin r}{\pi^2 - r^2} \sqrt{D(\chi)\, \mathrm{d}\chi}, \tag{15}$$

with

$$r = \frac{L}{2}\, \kappa(\omega) \cos(\chi).$$

Proof: Since the cost function in Eq. (12) is convex, it is sufficient to determine

$$\frac{\partial I(\eta_s, \eta_c)}{\partial \eta_s} = \frac{\partial I(\eta_s, \eta_c)}{\partial \eta_c} = 0 \tag{16}$$

in order to solve the optimization problem in Eq. (12). From $\frac{\partial I(\eta_s, \eta_c)}{\partial \eta_s} = 0$ we get

$$0 = 2 \int_{-L/2}^{L/2} \left(\int_0^\infty \int_{-\pi}^{\pi} \cos(\omega\, t - \kappa(\omega)\, X \cos(\chi) + \epsilon(\omega)) \sqrt{2\, S(\omega)\, D(\chi)\, \mathrm{d}\chi\, \mathrm{d}\omega} \right.$$
$$\left. - \eta_c(t) \cos\left(\frac{2\,\pi}{L}\, X\right) - \eta_s(t) \sin\left(\frac{2\,\pi}{L}\, X\right) \right) \sin\left(\frac{2\,\pi}{L}\, X\right) \mathrm{d}X$$

and it follows that

$$\eta_s(t) \int_{-L/2}^{L/2} \sin^2\left(\frac{2\,\pi}{L}\, X\right) \mathrm{d}X = \int_{-L/2}^{L/2} \int_0^\infty \int_{-\pi}^{\pi} \cos(\omega\, t - \kappa(\omega)\, X \cos(\chi) + \epsilon(\omega))$$
$$\sin\left(\frac{2\,\pi}{L}\, X\right) \sqrt{2\, S(\omega)\, D(\chi)\, \mathrm{d}\chi\, \mathrm{d}\omega}\, \mathrm{d}X. \tag{17}$$

The use of the trigonometric identity

$$\cos(\omega\, t + \epsilon(\omega) - \kappa(\omega)\, X \cos(\chi)) = \cos(\omega\, t + \epsilon(\omega)) \cos(-\kappa(\omega)\, X \cos(\chi))$$
$$- \sin(\omega\, t + \epsilon(\omega)) \sin(-\kappa(\omega)\, X \cos(\chi)) \tag{18}$$

in Eq. (17) leads to

$$\eta_s(t)\int_{-L/2}^{L/2}\sin^2\left(\frac{2\,\pi}{L}\,X\right)\mathrm{d}X = -\int_0^\infty \sin(\omega\,t+\epsilon(\omega))\sqrt{2\,S(\omega)\,\mathrm{d}\omega}$$
$$\int_{-\pi}^{\pi}\int_{-L/2}^{L/2}\sin\left(\frac{2\,\pi}{L}\,X\right)$$
$$\sin(-\kappa(\omega)X\cos(\chi))\,\mathrm{d}X\sqrt{D(\chi)\,\mathrm{d}\chi}.$$

Evaluating the integral with respect to X leads to

$$L\,\eta_s(t) = \int_0^\infty \sin(\omega\,t+\epsilon(\omega))\sqrt{2\,S(\omega)\,\mathrm{d}\omega}$$
$$\left(L\int_{-\pi}^{\pi}\frac{2\,\pi\sin\left(\frac{L}{2}\,\kappa(\omega)\cos(\chi)\right)}{\pi^2-\left(\frac{L}{2}\,\kappa(\omega)\cos(\chi)\right)^2}\,\sqrt{D(\chi)\,\mathrm{d}\chi}\right).$$

From this we obtain the resulting process $\eta_s(t)$ given in Eq. (13) after division by L. The determination of $\eta_c(t)$ is analogous. □

Accordingly, for the long-crested seas as given in equation (4), the following optimization problem has to be solved

$$\text{minimize}\quad I_{\mathrm{L}}(\eta_s,\eta_c) = \int_{-L/2}^{L/2}\left(Z_{\mathrm{L}}(X,0,t)-Z_{\mathrm{eff}}(X,Y,t)\right)^2\mathrm{d}X \tag{19}$$

This leads to the following result.

Theorem 3.2. *The solution of the optimization problem* (19) *is given by*

$$\eta_s(t) = \int_0^\infty f_s(\kappa(\omega))\sin(\omega\,t+\epsilon(\omega))\sqrt{2\,S(\omega)\,\mathrm{d}\omega}, \tag{20}$$

$$\eta_c(t) = \int_0^\infty f_c(\kappa(\omega))\cos(\omega\,t+\epsilon(\omega))\sqrt{2\,S(\omega)\,\mathrm{d}\omega}. \tag{21}$$

Thereby, the transfer functions f_s and f_c are given by

$$f_s(\kappa(\omega)) = \frac{2\,\pi\sin r}{\pi^2-r^2}, \qquad f_c(\kappa(\omega)) = \frac{2\,r\sin r}{\pi^2-r^2} \tag{22}$$

where $r = \frac{L}{2}\,\kappa(\omega)\cos(\chi_0)$.

Proof: In analogy to the proof of theorem 3.1, the optimal solution of (12) is given by

$$\frac{\partial I_{\mathrm{L}}(\eta_s, \eta_c)}{\partial \eta_s} = \frac{\partial I_{\mathrm{L}}(\eta_s, \eta_c)}{\partial \eta_c} = 0. \tag{23}$$

□

The comparison of the processes (13) and (14) with the irregular wave surface (3) shows that the spectral densities S_{η_c} and S_{η_s} of the respective stochastic processes η_c and η_s are related to the spectral density $S(\omega)$ of the irregular seas by

$$S_{\eta_s}(\omega) = S(\omega)\, f_s(\kappa(\omega))^2, \qquad S_{\eta_c}(\omega) = S(\omega)\, f_c(\kappa(\omega))^2 \tag{24}$$

The same relation applies accordingly to the processes (20) and (21) with the irregular long-crested wave surface $Z_{\mathrm{L}}(X, Y, t)$ given in equation (4). The spectrum of the process η_c determined by (22) from a JONSWAP spectrum, taking into account the encounter frequency (5), is shown in Fig. 2. Here the velocity U of the ship is 15 kn and the wave encounter angle χ_0 is 180°. A clear influence of the transfer function $f_c(\kappa(\omega))$ and the velocity U on the resulting spectral density $S_{\eta_c}(\omega)$ can be seen. Compared to the irregular wave elevation $Z(X, Y, t)$, the effective wave$Z_{\mathrm{eff}}(X, Y, t)$ has the great advantage that it depends only on the two parameters η_c and η_s or η and ψ. These are themselves stochastic processes with known spectral densities. If $\psi = 0$ or equivalently $\eta_s = 0$ is set in the equation (9), the effective wave simplifies to Grim's effective wave [6].

4. Modeling of nonlinear ship dynamics

Nonlinear equations of motion for ship dynamics using components of the effective wave are presented in this section. Thereby significant nonlinearities in roll damping and restoring are considered.

The nonlinear roll restoring moment of a ship is given by the righting lever curve GZ. For this purpose, the center of buoyancy B is calculated for relevant roll angles by integrating the pressure over the wetted surface of the ship hull. This is generally done by taking into account the pressure distribution of the incoming waves given by Bernoulli's equation.

As can be seen in Fig. 3, the slope of the function GZ with respect to the roll angle is larger in the wave trough than in the wave crest condition. This leads to higher initial stability of the upright floating position in the wave

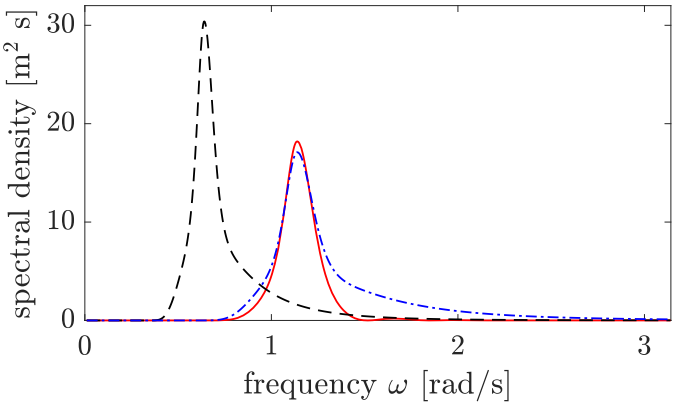

Figure 2: JONSWAP spectrum $S(\omega_0)$ (- - -), encounter JONSWAP spectrum $S_e(\omega)$ (-·-·-) and encounter spectral density $S_{\eta_c}(\omega)$ (——) for $H_s = 10$ m and $\omega_m = 0,64$ rad/s.

trough and reduced initial stability of the upright floating position in the wave crest compared to the ship stability in calm water. For conventional ships, the GZ curve approaches a global maximum for increasing roll angles φ. If the roll angle is increased further after reaching the global maximum, the righting arm GZ is reduced again for most ships until the GZ curve exhibits a zero crossing at the roll angle of vanishing stability and becomes negative thereafter. In calm water this angle of vanishing stability is denoted here by φ_s, as shown in Fig. 3. For a ship in a fixed wave, the angle of vanishing stability is generally different from φ_s. There are also cases where the ship is unstable at the wave crest, as can be seen from the dashed line in Fig. 3.

A vessel is considered as capsized when the maximum angle of vanishing stability in still water φ_s is exceeded. The velocity potential of the effective wave follows from linear wave theory, since the effective wave has a harmonic wave profile.

With the linearized Bernoulli equation [34] the space- and time-dependent pressure of the effective wave follows from the linear wave potential as

$$p_{\text{eff}} = \rho\, g\, \eta(t)\, \frac{\cosh\left(\frac{2\,\pi}{L}\,(Z+d)\right)}{\cosh\left(\frac{2\,\pi}{L}\,d\right)} \cos\left(\frac{2\,\pi}{L}\,X + \psi(t)\right) - \rho\, g\, Z. \tag{25}$$

Here, d is the water depth, $\eta(t)$ is the amplitude of the effective wave and $\psi(t)$ its phase. The temporal change in the righting lever curve caused by

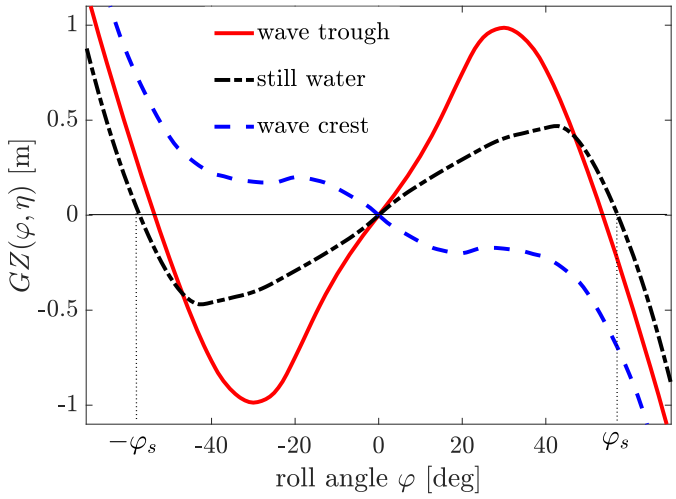

Figure 3: Righting arm GZ for different waves amidships.

the effective wave is a stochastic process because the amplitude η and phase ψ are stochastic processes.

If only relatively small heave and pitch motions compared to the roll motion are considered, a quasi-static consideration can be made. This means that the ship is in static equilibrium with respect to heave and pitch in the incoming waves. Then the function of the righting lever $GZ(\varphi, \eta, \psi, \chi)$ does not depend on the pitch and heave degrees of freedom. This significantly reduces the effort required to calculate the righting lever curve GZ, which is calculated for different roll angles φ of the ship in long-crested waves with wave heights η, cf. [1]. As also stated in [1], the resulting righting lever GZ is then approximated by the polynomial

$$GZ_{N_\varphi}(\varphi, \eta, \psi) = q_c\, \eta_c\, \varphi + \sum_{j=1}^{N_\varphi} q_j\, \varphi^j, \quad j \text{ odd}, \tag{26}$$

Whereby N_φ is the order of the polynomial. The form of Eq. (26) was obtained in [1] from fitting a functional expression to the righting lever GZ.

Using the above considerations, the rolling behavior of the ship can be

determined by means of the following equation of motion

$$(I_{xx} + A_{xx})\,\ddot{\varphi} + b_1\,\dot{\varphi} + b_2\,\dot{\varphi}\,|\dot{\varphi}| + b_3\,\dot{\varphi}^3 + g\,\Delta\,GZ_{N_\varphi}(\varphi, \eta, \psi) = M. \tag{27}$$

In this equation, I_{xx} is the roll inertia, A_{xx} is the hydrodynamic added inertia evaluated at the damped natural frequency of roll, b_1, b_2, and b_3 are roll damping coefficients, g is acceleration due to gravity, Δ is the displacement, and $M(\eta, \psi)$ is an external roll moment. This model is studied in detail in [1, 5]. From Eq. (27) in combination with Eq. (26) we can see that $\eta_c(t)$ leads to parametric forcing due to incident waves. With this observation, the random process $\xi_2(t)$ due to parametric wave excitation in Eq. (27) is given by

$$\xi_2(t) := \eta_c(t). \tag{28}$$

In order to determine the external roll moment $M(\eta, \psi)$, we adapt a common approximation procedure, e.g. [35]. In this procedure, the wave profile of the effective wave perpendicular to ship forward direction is approximated by a straight line. This line is inclined by the angle

$$\begin{aligned} \varphi_e(t) &= \arctan\left(-\frac{2\pi}{L}\sin(\chi_0)\eta(t)\sin(\psi(t))\right) \\ &= \arctan\left(\frac{2\pi}{L}\sin(\chi_0)\eta_s(t)\right). \end{aligned} \tag{29}$$

In Eq. (29) the wave length L is much larger than the wave amplitude $\eta(t)$. Therefore, we can use the linear approximation of arctan in Eq. (29), which leads to

$$\varphi_e(t) \approx \frac{2\pi}{L}\sin(\chi_0)\eta_s(t). \tag{30}$$

The excitation moment is then obtained from the still water righting lever GZ_{still} as

$$M(\eta, \psi) = \Delta g GZ_{\text{still}}(\varphi_e(t)). \tag{31}$$

Again, we consider the fact that φ_e is small and use a linear approximation $GZ_{\text{still}}(\varphi_e) = q_0\varphi_e$, which results in

$$M(\eta, \psi) = \Delta g q_0 \frac{2\pi}{L}\sin(\chi_0)\eta_s(t). \tag{32}$$

Thus the random process $\xi_1(t)$ involved in the roll moment is given by

$$\xi_1(t) := \eta_s(t). \tag{33}$$

A good choice for q_0 in Eq. (32) is to set q_0 to be equal to the metacentric height GM. However, one can also fit the still water righting lever GZ_{still} up to the maximal possible angle $\max(\varphi_e(t))$. The frequency of excitation due to the external roll moment is the frequency of wave encounter ω (cf. [36]).

As a result, the second order differential equation (27) yields the first order system for the rolling motion

$$\begin{aligned} \dot{u} &= v, \\ \dot{v} &= \sum_{j=1}^{N_\varphi} \bar{\alpha}_j \, u^j - \bar{\beta}_1 \, v - \bar{\beta}_2 \, v \, |v| - \bar{\beta}_3 \, v^3 + \bar{\nu}_1 \, \xi_1 + \bar{\nu}_2 \, \xi_2 \, u, \end{aligned} \tag{34}$$

whereby the coefficients are given by

$$\bar{\beta}_i = \frac{b_i}{I_{xx} + A_{xx}}, \qquad \bar{\nu}_2 = \frac{q_c}{I_{xx} + A_{xx}}, \; \bar{\alpha}_j = -\frac{g \, \Delta}{I_{xx} + A_{xx}} \, q_j, \quad j \text{ odd}. \tag{35}$$

Moreover, ν_1 is the noise intensity due to the external roll moment and ν_2 is the noise intensity due to the parametric forcing obtained from the fitting of the parameter q_c in Eq. (26). If the external roll moment according to Eq. (32) is used, then ν_1 is given by

$$\bar{\nu}_1 = \frac{\Delta g q_0 \frac{2\pi}{L} \sin(\chi_0)}{I_{xx} + A_{xx}}.$$

We introduce the small scaling parameter ε which is important for the application of stochastic averaging described in section 5. With this, the rescalings of ship parameters and time t are obtained as

$$\begin{aligned} &u = x, \quad v = \varepsilon \, y, \quad \bar{\alpha}_j = \varepsilon^2 \, \alpha_j, \quad \bar{\beta}_1 = \varepsilon^2 \, \beta_1, \\ &\bar{\beta}_2 = \varepsilon \, \beta_2, \quad \bar{\beta}_3 = \beta_3, \quad \bar{\nu}_1 = \varepsilon^{\frac{5}{2}} \, \nu_1, \quad \bar{\nu}_2 = \varepsilon^{\frac{5}{2}} \, \nu_2, \quad t_\varepsilon = \varepsilon \, t. \end{aligned} \tag{36}$$

This leads to the equations of motion

$$\begin{aligned} \frac{\mathrm{d}}{\mathrm{d}t_\varepsilon} x &= y, \\ \frac{\mathrm{d}}{\mathrm{d}t_\varepsilon} y &= \sum_{j=1}^{N_\varphi} \alpha_j \, x^j - \varepsilon \, (\beta_1 \, y + \beta_2 \, y \, |y| + \beta_3 \, y^3) + \sqrt{\varepsilon} \, (\nu_1 \, \xi_1(t_\varepsilon) + \nu_2 \, x \, \xi_2(t_\varepsilon)). \end{aligned} \tag{37}$$

The corresponding undisturbed equations of motion form a Hamiltonian system and are given by

$$\begin{aligned} \frac{\mathrm{d}}{\mathrm{d}t_\varepsilon} x &= y, \\ \frac{\mathrm{d}}{\mathrm{d}t_\varepsilon} y &= \sum_{j=1}^{N_\varphi} \alpha_j \, x^j. \end{aligned} \tag{38}$$

In analogy to the results obtained in [5, 37], the Eq. (34) can be restated as a weakly perturbed Hamiltonian system, with Hamiltonian

$$H(x, y) := \frac{y^2}{2} + U(x), \tag{39}$$

where

$$U(x) = -\sum_{j=1}^{N_\varphi} \frac{\alpha_j}{j+1} \, x^{j+1} \tag{40}$$

is the potential energy, x is the roll angle, y is the scaled roll velocity, and α_j are real coefficients. For $y \geq 0$ we then obtain the following system of differential equations for the roll energy H and scaled roll angle x on scaled time $t_\varepsilon = \varepsilon t$

$$\begin{aligned} \frac{d}{dt_\varepsilon} x &= \sqrt{Q(x, H)}, \\ \frac{d}{dt_\varepsilon} H &= \varepsilon Q(x, H) G(x, H) + \sqrt{\varepsilon} \sqrt{Q(x, H)} \big(\nu_1 \xi_1(t_\varepsilon) \\ &\qquad + x \nu_2 \xi_2(t_\varepsilon) \big), \end{aligned} \tag{41}$$

with

$$Q(x, H) := 2H + \sum_{j=1}^{N_\varphi} \frac{2\alpha_j}{j+1} \, x^{j+1} \tag{42}$$

and

$$G(x, H) := (-\beta_1 - \beta_2 \sqrt{Q(x, H)} - \beta_3 Q(x, H)). \tag{43}$$

For $y < 0$ we get in analogy

$$\begin{aligned} \frac{d}{dt_\varepsilon} x &= -\sqrt{Q(x, H)}, \\ \frac{d}{dt_\varepsilon} H &= \varepsilon Q(x, H) G(x, H) - \sqrt{\varepsilon} \sqrt{Q(x, H)} \big(\nu_1 \xi_1(t_\varepsilon) \\ &\qquad + x \nu_2 \xi_2(t_\varepsilon) \big). \end{aligned} \tag{44}$$

The parameter ε is much smaller than one, since hydrodynamic damping and excitation due to sea are small compared to the restoring force of a ship. The period $T(H)$ of one oscillation of fast variable x in the absence of noise and damping, i.e. $\varepsilon = 0$, starting at an energy level H of a non-capsized case is given by

$$T(H) = 2 \int_{-b(H)}^{b(H)} \frac{dx}{\sqrt{Q(x, H)}}, \tag{45}$$

where $b(H)$ denotes the roll amplitude at energy level H. A relation between H and b can be obtained by substituting $x = b$ into the equation $\sqrt{Q(x, H)} = 0$ and solving for b. For a cubic roll restoring nonlinearity the relation between the roll energy H and the roll amplitude b(H) is given in Eq. (A.3) in the appendix.

The state variables x and H in system (41) exhibit two different time scales, since the roll energy H changes slowly with time compared to the change of the variable x.

5. Energy-based stochastic averaging

Following the energy-based stochastic averaging method described in Dostal et al. [5], the system of scaled roll angle x and energy H in Eqs. (41) and (44) can be reduced to a one-dimensional process of the energy H. This is important in order to efficiently determine mean first passage times in the next section.

The result is that, as ε converges to zero, the energy process H converges weakly to a one-dimensional Markov process H_0 which is governed by the Itô equation

$$dH_0 = m(H_0)dt + \sigma(H_0)dW_t. \tag{46}$$

For brevity, we use H instead of H_0 in the following to denote the averaged process of energy H (note that H_0 is the stochastic averaging result of the energy H stated in Eq. (39)). In the above Itô Eq. (46), $m(H)$ denotes the drift and $\sigma(H)$ the diffusion of the energy process H. Following the procedure for the energy based stochastic averaging method as described in [5, 38] and using a formulation such that arbitrary nonlinearities in the roll restoring

can be used leads to the the drift

$$\begin{aligned} m(H) =& \frac{1}{T(H)} \int_{-\infty}^{0} \Big\{ R_{\xi_1\xi_1}(\tau)\nu_1^2 \int_0^{T(H)} \frac{y_H(s+\tau)}{y_H(s)} ds \\ &+ R_{\xi_2\xi_2}(\tau)\nu_2^2 \int_0^{T(H)} x_H(s)\, x_H(s+\tau) \frac{y_H(s+\tau)}{y_H(s)} ds \Big\}\, d\tau \\ &- \frac{1}{T(H)} \int_0^{T(H)} y_H^2(s)(\beta_1 + \beta_2 |y_H(s)| + \beta_3 y_H^2(s)) ds \end{aligned} \tag{47}$$

and the diffusion

$$\begin{aligned} \sigma^2(H) =& \frac{1}{T(H)} \int_{-\infty}^{\infty} \Big\{ R_{\xi_1\xi_1}(\tau)\nu_1^2 \int_0^{T(H)} y_H(s) y_H(s+\tau) ds \\ &+ R_{\xi_2\xi_2}(\tau)\nu_2^2 \int_0^{T(H)} x_H(s)\, x_H(s+\tau) y_H(s) y_H(s+\tau)\, ds \Big\}\, d\tau, \end{aligned} \tag{48}$$

where $R_{\xi_i\xi_i}(\tau) = E\{\xi_i(\tau + t)\xi_i(t)\}$ are the autocorrelation functions of the processes ξ_i, $i = 1, 2,$. The states $x_H(s)$ and $y_H(s)$ are obtained from the undisturbed equation of motion

$$\begin{aligned} \frac{\mathrm{d}}{\mathrm{d}s} x_H &= y_H, \\ \frac{\mathrm{d}}{\mathrm{d}s} y_H &= \sum_{j=1}^{N_\varphi} \alpha_j\, x_H^j, \end{aligned} \tag{49}$$

whereby the initial condition is given by $x_H(0) = 0$, $y_H(0) = \sqrt{2H}$, such that trajectories with constant energy H are generated.

For $N_\varphi = 3$ and $N_\varphi = 5$, explicit formulas for the drift m and diffusion σ are given in Appendix A. For higher order polynomial nonlinearity $N_\varphi > 5$, the drift $m(H)$ and diffusion $\sigma(H)$ can be obtained by numerically determining $x_H(s)$ and $y_H(s)$ from Eq. (49). From these numerical results, also the period $T(H)$ and the response amplitude $b(H)$ of the roll motion can be obtained.

In order to apply the energy based stochastic averaging for the ship roll equations of motion from Eq. (37), the following assumptions have to be fulfilled.

First of all, it is assumed that the random forcing ξ_1 and ξ_2 in Eq. (37) are Gaussian processes and satisfy the condition of strong mixing, as further described in [39] and references therein. Strong mixing of the random process ξ roughly means that the dependence between $\xi(t)$ and $\xi(t+\tau)$ decreases sufficiently fast as τ increases. This is for example the case if ξ is a wide band random process. This is fulfilled for many sea states. However, one has to be careful with some encounter sea states, which can get very narrow band.

Moreover, in our analysis we are focusing on the non-capsized case and therefore assume that a stationary probability density exists. This means that the energy H does not exceed the critical energy H_c corresponding to the angle of vanishing stability φ_s in still water. The critical energy H_c for the assumed condition $H < H_c$ is obtained by

$$H_c = U(\varphi_s). \tag{50}$$

The stationarity assumption implies together with the scaling introduced in Eq. (37), where ε is a small parameter, that the response variance is finite, cf. [40, 18]. It should be noted that the assumption of the non-capsized case is not a loss of generality for the application of stochastic averaging to this problem, but makes the procedure easier to follow. The reason is that it is possible to extend the current stochastic averaging procedure to include the non-capsized as well as the capsized case. But then the introduction of gluing conditions and another set of averaged equations is necessary according to the stochastic averaging procedure described in Namachchivaya [41], which among others includes the theory on large deviations and averaging developed by Freidlin and Wentzell, e.g. [42, 43].

Finally, as indicated by the ε-scaling in the equations of motion Eq. (37), we assume small damping and forcing, such that during typical oscillation cycles of period $T(H)$ the trajectories of Eq. (37) are close to the trajectories of the undisturbed Hamiltonian system given by Eq. (38). This assumption is also met by many ships and not too severe sea states.

A study on the effect of stronger damping, stronger forcing intensity and narrow band excitation on the results of stochastic averaging for ships in random seas can be found in [44]. For severe sea states Monte Carlo simulation, as described in the next section, can be used for the determination of first passage times, since in this case the first passage times are lower and consequently the computation time using Monte Carlo simulation is also lower

than in moderate or low wave sea states. However, for sea states with low or moderate significant wave heights, the computation time of first passage times using Monte Carlo simulations can be of several orders of magnitude higher, especially for low wave heights. Then the proposed approach using stochastic averaging together with the formulas for first passage times from the next section 6 is much more efficient, as is also shown in section 6.

Another method of stochastic averaging of energy envelope was already published by J. B. Roberts in [45, 46].

In contrast to the stochastic averaging of the equations of motion stated above in Eqs. (41) and (44), different equations of motions involving the total energy H and an associated phase process Φ are averaged [47, 14]. These equations are obtained using the transformation

$$\begin{aligned} \operatorname{sgn}(x)\,\sqrt{U(x)} &= \sqrt{H}\cos\Phi, \\ \dot{x} &= -\sqrt{2\,H}\sin\Phi, \end{aligned} \tag{51}$$

where $U(x)$ is the potential energy, cf. Eq. (40). The resulting equations of motion are

$$\begin{aligned} \dot{H} &= \varepsilon\, 2Hh\sin^2\Phi - \sqrt{\varepsilon}\,\sqrt{2\,H}\,\sin\Phi\,\nu_1\,\xi_1, \\ \dot{\Phi} &= \varepsilon\, h\cos\Phi - \sqrt{\varepsilon}\,\frac{\cos\Phi}{\sqrt{2\,H}}\,\nu_1\,\xi_1 - \gamma, \end{aligned} \tag{52}$$

where

$$h = -\beta_1 - \sqrt{2\,H}\,\beta_2\sin\Phi - 2\,H\,\beta_3\sin^2\Phi, \tag{53}$$

$$\gamma = \frac{\left|\sum_{j=1}^{N_\varphi}\alpha_j\,x^j\right|}{U(x)}. \tag{54}$$

As described by Roberts and Vasta in [18], the initial energy based stochastic averaging approach derived by J. B. Roberts in [45, 46] made use of a non-consistent approximation with respect to the γ term in Eq. (52), which is not based on theoretical foundations. In order to fix this issue, Roberts and Vasta have improved the previous results from [45, 46] using Tailor series approximations, as shown in [17, 18].

In comparison with the improved energy based stochastic averaging approach by Roberts and Vasta in [17, 18], the energy-based stochastic averaging method used in this work is based on the equations of motion in Eqs. (41) and (44), which are in the required form for the application of

stochastic averaging and thus no additional approximations using Taylor series expansions are necessary as done in [17, 18]. This makes the resulting expressions simpler and more accurate than the improved averaging procedure derived by Roberts and Vasta. Moreover, parametric excitation was not considered by Roberts and Vasta in [17, 18]. This should however be possible without problems.

6. First passage times

With the above considerations, the mean first passage time for the one-dimensional process of roll energy H, given by the Itô equation

$$dH = m(H)dt + \sigma(H)dW_t, \tag{55}$$

can be determined, whereby the process H is defined in the interval $[H_l, H_r]$ with boundaries H_l and H_r. But first it is necessary to introduce some measures, as well as a *regular boundary* and an *exit boundary* of the one-dimensional diffusion process of the roll energy H. Following [48, 23], the *scale measure* of Eq. (55) is defined by

$$S(x) = \int_{x_0}^{x} s(\zeta)d\zeta, \tag{56}$$

where

$$s(\zeta) = \exp\left(-2\int_{\zeta_0}^{\zeta} \frac{m(y)}{\sigma^2(y)}dy\right)$$

is the *scale density* and x_0, ζ_0 are arbitrary interior points $x_0, \zeta_0 \in (H_l, H_r)$. Moreover, the *speed measure* is defined by

$$M[c, d] = \int_{c}^{d} \mu(x)\mathrm{d}x, \tag{57}$$

with the *speed density*

$$\mu(x) = 1/(\sigma^2(x)s(x)). \tag{58}$$

Then, as stated in [48], a right boundary H_r of the one-dimensional diffusion process $H \in [H_l, H_r]$ is said to be an *exit boundary*, if the time T_r to reach the boundary H_r from an interior point is finite and if the speed measure fulfills the condition

$$M[H, H_r) = \lim_{a \to H_r} M[H, a] = \infty. \tag{59}$$

Hereby, $M[H, H_r)$ measures the speed of the process H near the boundary H_r. In other words, the process H can leave the *exit boundary* and can not come back any more. Physically this is the case of a capsized ship which can not get back to its upright position again. In addition, a boundary is *regular*, if the diffusion process can both enter and leave this boundary.

It is possible in certain cases to find explicit solutions of the mean first passage times. The case relevant to the energy of nonlinear oscillators was studied by Dostal and Sri Namachchivaya in [23], where closed form formulas are derived based on solutions of Pontryagin's equation. These results can be used to determine the required first-passage times of the roll energy H, which leads to the following theorem.

Theorem 6.1. *Let the time evolution of the roll energy H be a solution of the one-dimensional Itô equation (55) and let the boundary at the point H_c be a regular or an exit boundary. Then the mean time for reaching the point H_c for the first time starting from the initial roll energy $H_i \in [0, H_c]$ is given by*

$$M_1(H_i) = 2 \int_{H_i}^{H_c} \left[\int_z^{H_c} s(y)\,\mathrm{d}y \right] \mu(z)\,\mathrm{d}z + 2 \int_{H_i}^{H_c} s(y)\,\mathrm{d}y \int_0^{H_i} \mu(z) dz \quad (60)$$

and $M_1(H_i) < \infty \;\forall\; H_i \in [0; H_c]$. Note, that here the minimal possible roll energy is normalized to $H_{\min} = 0$.

The proof of Theorem 6.1 is presented in [23].

6.1. Reference ship

In order to evaluate the proposed procedure of determination of first passage times according to Eq. (60), the ship presented by Krüger et al. in [49] is exemplary used. This ship is susceptible for large amplitude parametric roll dynamics and has significant nonlinearities in its righting arm GZ. This ship is an about 200 m long RoRo ferry with four cargo decks. The side view of the hull of this RoRo vessel can be seen in Fig 4. The corresponding frames are shown in Fig 5. Furthermore, the main dimensions of the ship are shown together with data from a critical loading case with a GM of 1.05 m are summarized in Tab. 1.

Using the data from table 1, the lever arm curves GZ of the RoRo ship were determined for the wave crest and wave trough situations, as well as for smooth water at waves of length $L = 205$ m. The resulting lever arm curves

Table 1: Data of the considered RoRo ship.

length between perpendiculars	L_{pp}	$189,70$	m
beam	B	$26,50$	m
draft	T	$6,95$	m
displacement	Δ	20400	t
roll radius of gyration	i_{xx}	$21,347$	m
roll moment of inertia	$I_{xx} + A_{xx}(\omega_n)$	$9,668 \cdot 10^6$	t m^2
roll eigenfrequency	ω_n	$0,1496$	rad/s
Service speed	v_s	$22,4$	kn

are shown in Fig 3. From these lever arm curves, it can be seen that this ship can be considered capsized at roll amplitudes of 68° and above, since the lever arms are negative for positive roll angles in all wave situations.

For the considered RoRo ship, the following velocity dependent roll damping function is used

$$d(\dot{\varphi}) = \beta_1(U)\,\dot{\varphi} + \beta_2(U)\,\dot{\varphi}\,|\dot{\varphi}|, \tag{61}$$

whereby the ship velocity is denoted by U. Moreover, the velocity-dependent coefficients $\beta_1(U)$ and $\beta_2(U)$ shown in Fig. 6 are used according to the description in [50]. The remaining coefficients of the equations of motion (34) for the RoRo ship are given in table 2, whereby the righting lever is approximated using polynomial of the order $N_\varphi = 3$.

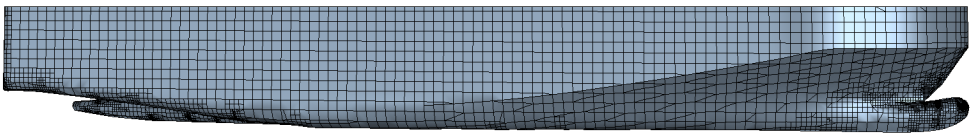

Figure 4: Side view of the RoRo ship.

6.2. Mean first passage times of critical roll energy

In order to present the proposed approach, mean first-passage times are determined for the considered RoRo ship according to Theorem 6.1. The

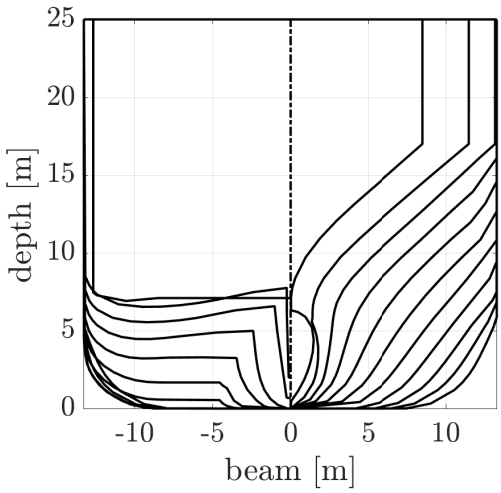

Figure 5: Frames of the RoRo ship.

Table 2: Coefficients of considered RoRo ship

	$\bar{\alpha}_1 = 0.037029$	$\bar{\alpha}_3 = 0.057132$	$\bar{\nu}_2 = 0.007705$
$\varepsilon = 0.1$	$\alpha_1 = 3.7029$	$\alpha_3 = 5.7132$	$\nu_2 = 2.43657$

loading condition studied in [49] with a GM of 1.05 m and JONSWAP sea states with significant wave heights H_s of three to ten meters at a mean sea state period of $T_1 = 11.5$ s are used. Also, a critical roll amplitude of 30° is chosen. At roll amplitudes greater than 30°, cargo shifting and loss of containers are possible, which then leads to a change in the position of the ship's center of gravity so that the upright floating position of the ship is no longer stable. Furthermore, injuries to passengers and crew are very likely with such large roll amplitudes. Moreover, an instantaneous roll angle of 30° for a RoRo ferry can be considered a criterion for capsize, as is stated by "IMO 76/23" and by "ITTC Recommended practices and guides - Numerical simulation of capsize behavior of damaged ships in irregular seas". Using the proposed method for the considered RoRo ship, Fig. 7 shows the mean first passage time results of reaching the critical roll amplitude $\varphi_c = 30°$ starting at the initial roll amplitude $\varphi_0 = 5°$ for the wave encounter angle $\chi_0 = 5°$, significant wave height H_s, and ship speed U.

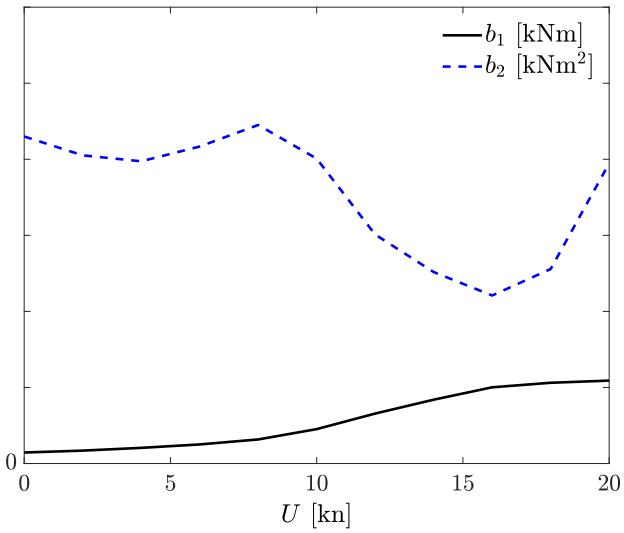

Figure 6: Qualitative representation of the ship's damping coefficients.

The results presented in Fig. 7 clearly show the parametric 2:1 resonance phenomenon at a ship speed U of about 3.7 kn, where the wave encounter frequency is close to twice the roll natural frequency. The mean time to reach the critical roll amplitude $\varphi_c = 30°$ at this speed and a significant wave height of $H_s = 3$ m is just about 50 minutes. If this resonance condition is not met, the times to exceed the critical roll amplitude for the first time can be very long and thus exceeding the critical roll amplitude φ_c is very unlikely, as is the case in the yellow regions of Fig. 7.

6.3. Comparison with numerical simulation

Determining corresponding results as shown in Fig. 7 using numerical simulations is very time consuming. In order to determine the mean of a first passage time which is about one year, illustrative a much higher simulation time of about 100 years has to be used until 100 crossings are reached, in order to obtain an accurate mean value for such one specific case. Otherwise, the obtained mean value might not be very accurate. Keeping this in mind, we have set up numerical simulations for the determination of mean first passage times using the following considerations:

1.) For each desired combination of significant wave height H_s and ship

speed U, the roll motion of the ship is simulated until the critical roll angle φ_c is reached, starting at initial conditions for roll angle φ_0 and roll velocity $\dot{\varphi}_0$. The corresponding initial roll energy can be obtained from Eq. (39) if setting $x = \varphi_0$ and $y = \dot{\varphi}_0$. Then the corresponding time t_i $(i = 1, 2, ..., m)$ is stored and the simulation is restarted at the initial conditions φ_0 and $\dot{\varphi}_0$.

2.) The termination condition of the simulation procedure in 1.) is set to be either a maximal total simulation time of $T_m = 5$ years or a maximal number of $n = 100$ crossings of the critical roll angle φ_c.

3.) The mean first passage time M_1 for each simulation case is then obtained from the stored times t_i by $M_1 = \frac{1}{m}\sum_{i=1}^{m} \delta t_i$, where $\delta t_i = t_i - t_{i-1}$ is the time between two consecutive crossings of φ_c. Note, that the number m of times t_i can be smaller than the maximal number $n = 100$ of crossings of φ_c, if φ_c is reached less than n times during the total simulation time.

Using the described simulation procedure, we have computed the simulated mean first passage time for the same case as considered in Sec. 6.2, where $\varphi_c = 30°$, $\chi_0 = 5°$, $\varphi_0 = 5°$, $\dot{\varphi}_0 = 0$, using the JONSWAP sea state with significant wave height H_s and mean wave period $T_1 = 11.5$ s. These simulation results of mean first-passage times are shown in Fig. 8. The white regions in Fig. 8 denote mean first passage times larger than 5 years, which were not obtained using numerical simulations.

In addition, the number m of crossings of the critical angle φ_c encountered during the numerical simulation results is shown in Fig. 9 for each combination of U and H_s. For only three cases in Fig. 9 the number of crossings m lies between $m = 1$ and $m = 99$. For the rest of the considered cases the number of crossings is either $m = 100$ or $m = 0$.

For better comparison with the numerical results, we have re-plotted the mean first passage times obtained using the proposed method from Sec. 6.2 in Fig. 10, where the white regions also denote mean first passage times larger than 5 years. In comparison with the results from Fig. 10 using the proposed first passage time formula in Eq. (60), the mean first passage times of the numerical simulation results from Fig. 8 are slightly shifted to the left in comparison with the results from Fig. 10 for ship speeds larger than $U = 4$ kn. For ship speeds below $U = 4$ kn the mean first passage time

results from Fig. 10 and 8 agree well. The reasons for this have to be studied further in future research.

However, the computation times differ significantly. According to the numerical simulation procedure from this subsection, the computation time of the mean first passage times is roughly proportional to the resulting mean first passage time, depending on the factor f_c between numerically simulated time and the computation time. It also depends on the reached number m of crossings of the critical angle φ_c during the simulation. A formula for the estimation of the computation time Θ_c of mean first passage times M_1 using the numerical simulation procedure can be stated as

$$\Theta_c = f_c \, m \, M_1 \tag{62}$$

We have used a computer with the computation time factor $f_c = 0.00235$ on one processor core. The resulting computation time of the mean first passage times $\Theta_{0.001}$ of 0.001 years and $m = 100$ crossings is therefore $\Theta_{0.001} = 2.0586$ hours. For $m = 100$ and the mean first passage time of 0.1 years we get $\Theta_{0.1} = 205.86$ hours and for the mean first passage time of 1 year we consequently get $\Theta_1 = 2058.6$ hours.

The computation time of the mean first passage time using the presented method is only several minutes for each computed case on one processor core. Therefore, the difference between the computation time for the presented method and the computation time for numerical simulations can be huge.

Using the numerical simulation procedure described in this subsection, the computation time to obtain the results shown in Fig. 8 required about *two weeks on 12 cores* of standard desktop computers. Whereas applying the proposed theory using the formula Eq. (60) in Theorem 6.1, the computation time for the results shown in Fig. 10 is about *10 hours on one core* of a standard desktop computer. This is about 400 times faster.

6.4. Variation of the center of mass

The vertical position of the center of mass of the ship can be stated in terms of the distance KG from the keel to the center of mass. The distance KG affects the righting lever curve GZ and thus the stability of the ship. This also affects the corresponding mean first passage times. For the considered RoRo ship, a loading condition with $KG = 13.1$ m results in the metacentric height $GM = 1.05$ m with a draft of 7 meters. For this loading condition, the current IMO intact stability criteria are satisfied. However, from the numerical stability assessment according to Krüger and Hatecke [49], a minimum

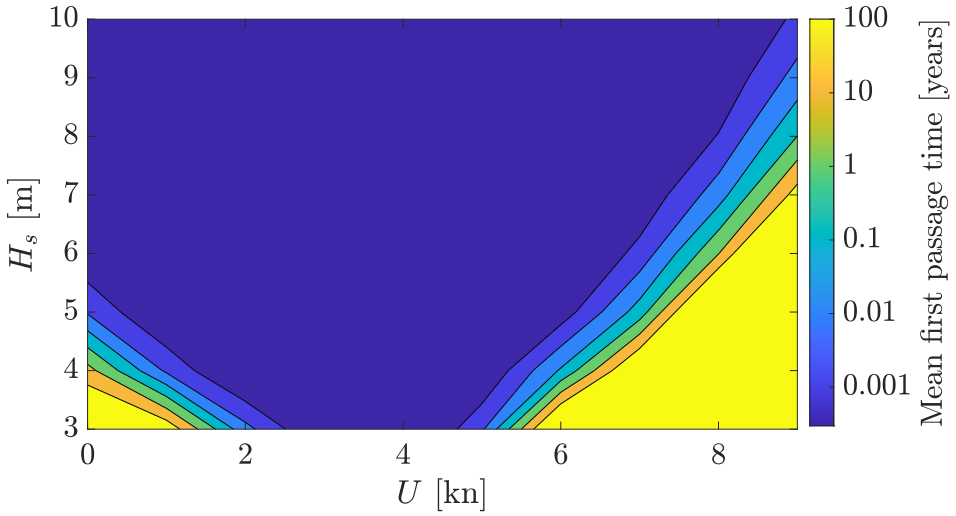

Figure 7: Full mean first-passage times of roll amplitude $\varphi_c = 30°$ for wave encounter angle $\chi_0 = 5°$, ship speed U, and JONSWAP sea state with significant wave height H_s and mean wave period $T_1 = 11.5$ s.

value for the metacentric height of $GM = 1.4$ m turns out to be necessary to ensure stability of the RoRo ship. Thus, the KG range between 12.6 m and 13.8 m is critical for the stability assessment of the RoRo ship. The contour lines of the mean first passage times for reaching the roll amplitude $\varphi_c = 30°$for different KG and ship velocities U are shown in Fig. 11 for the case of wave encounter angle $\chi_0 = 5°$, JONSWAP sea state with mean wave period $T_1 = 11.5$ s, and significant wave height H_s= 3 m . As the natural frequency of the roll oscillation becomes smaller for larger KG values, the ship velocity U at which the 2:1 resonance condition for parametric roll is reached also changes, which can be observed in this figure.

The results shown in Figs. 10 to 11 contain regions with very large mean first-passage times. Numerical simulation has so far only been able to determine areas with short mean first-passage times of the critical roll amplitude. This is due to the fact that for each parameter combination several simulation runs are necessary to simulate statistically relevant data for the determination of the mean first passage time. In order to save computation time, the determination of the mean first passage times is often omitted. Instead, fixed time periods are chosen in which the rolling motion is simulated. However,

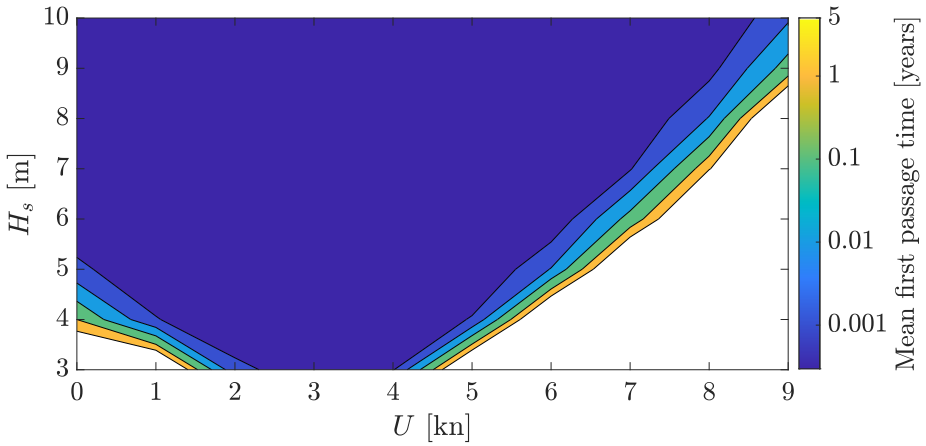

Figure 8: Simulation results of mean first-passage times of roll amplitude $\varphi_c = 30°$ for wave encounter angle $\chi_0 = 5°$, ship speed U, and JONSWAP sea state with significant wave height H_s and mean wave period $T_1 = 11.5$ s.

using the proposed approach using Theorem 6.1, computation of mean first passage times for ship roll motion becomes feasible.

7. Conclusions

With the proposed approach, the mean first passage time of roll motion of ships to reach critical roll angles is obtained, which is important for the determination of dangerous ship roll dynamics in ocean waves. This is done by first determining a one-dimensional diffusion process for the roll energy. Then, analytical results for the determination of mean first passage times, as described in section 6, are used to obtain the desired mean first passage times for critical roll energy.

Using the proposed approach, the required computation time is much lower compared to numerical simulations, since the proposed analytical expressions for the mean first passage times in integral form can be evaluated using standard quadrature formulas. This is important for the design of ships, where many different random sea conditions with waves from different directions have to be calculated. Moreover, it is possible to determine mean first-passage times that are significantly larger than the mean first-passage times that can be determined using numerical simulation in reasonable time.

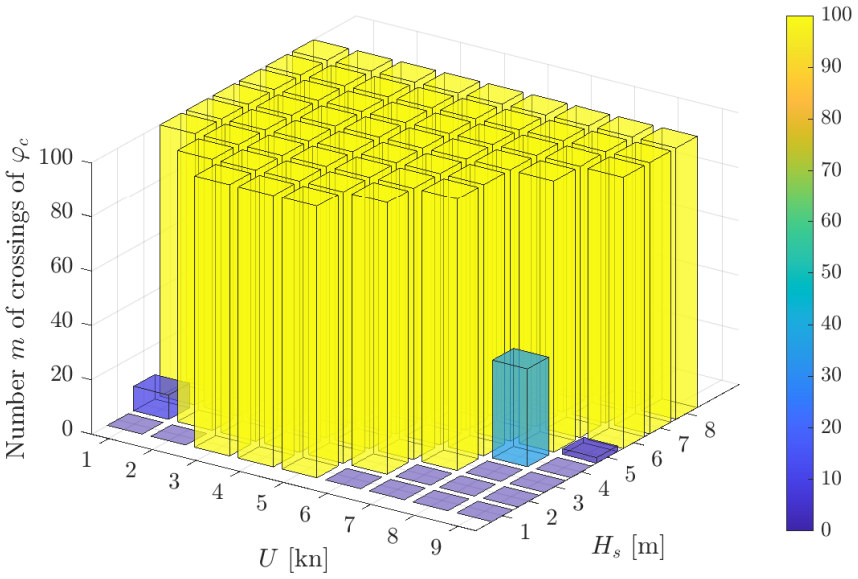

Figure 9: Histogram of crossings m of roll amplitude $\varphi_c = 30°$ according the procedure from subsection 6.3 for wave encounter angle $\chi_0 = 5°$, ship speed U, and JONSWAP sea state with significant wave height H_s and mean wave period $T_1 = 11.5$ s.

This leads to new results that can be used to evaluate the nonlinear dynamics of ships in real sea states.

Appendix A. Averaging formulas

For the case, where the righting lever curve GZ in Eq. (26) can be approximated by a cubic polynomial with $N_\varphi = 3$, reduced expressions for the drift and diffusion of the roll energy are determined in[5]. Using these results for the non-capsized case, where $0 \leq H < \frac{\alpha_1^2}{4\alpha_3}$, the drift $m(H)$ in Eq. (47)

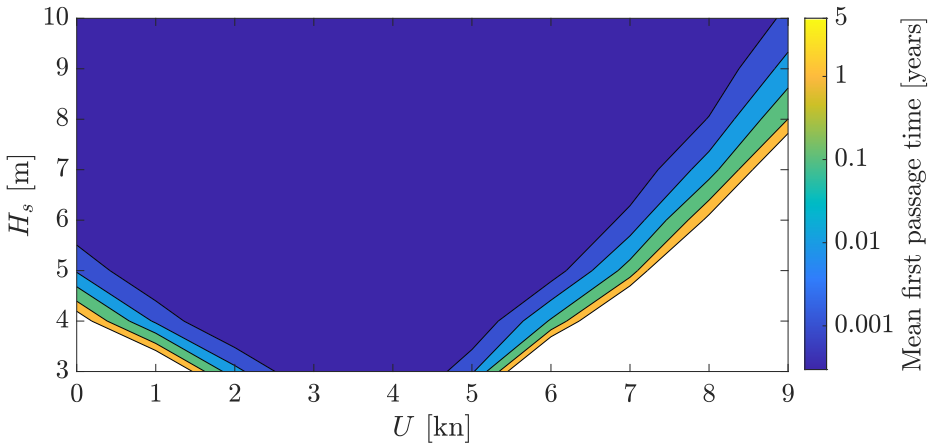

Figure 10: Mean first-passage times of roll amplitude $\varphi_c = 30°$ for wave encounter angle $\chi_0 = 5°$, ship speed U, and JONSWAP sea state with significant wave height H_s and mean wave period $T_1 = 11.5$ s.

and diffusion $\sigma(H)$ in Eq. (48) can be further reduced to

$$\begin{aligned} m(H) =& \frac{2}{Tq}\int_{-\infty}^{0}\Big\{R_{\xi_1\xi_1}(\tau)\nu_1^2\int_{-K(k)}^{K(k)}\frac{cn_{t+\tau}dn_{t+\tau}}{cn\,dn}du+ \\ &+ R_{\xi_2\xi_2}(\tau)b^2\nu_2^2\int_{-K(k)}^{K(k)} sn\;sn_{t+\tau}\frac{cn_{t+\tau}dn_{t+\tau}}{cn\,dn}du\Big\}\,d\tau+ \\ &+ \frac{1}{T}\int_0^T Q(x(t),H)G(x(t),H)dt, \end{aligned} \tag{A.1}$$

$$\begin{aligned} \sigma^2(H) =& \frac{4b^2q}{T}\int_{-\infty}^{\infty}\Big\{R_{\xi_1\xi_1}(\tau)\nu_1^2\int_0^{K(k)} cn\;dn\;cn_{t+\tau}\;dn_{t+\tau}du+ \\ &+ R_{\xi_2\xi_2}(\tau)b^2\nu_2^2\int_0^{K(k)} sn\;sn_{t+\tau}cn\;dn\;cn_{t+\tau}\;dn_{t+\tau}\;du\Big\}\,d\tau \end{aligned} \tag{A.2}$$

The above expressions contain the variables

$$\begin{aligned} b =& \sqrt{-\frac{-\alpha_1+\sqrt{\alpha_1^2-4\alpha_3 H}}{\alpha_3}}, \quad a = \sqrt{\frac{4H}{b^2\alpha_3}}, \\ q =& a\sqrt{\frac{\alpha_3}{2}}, \quad T(H) = \frac{4}{q}K(k), \end{aligned} \tag{A.3}$$

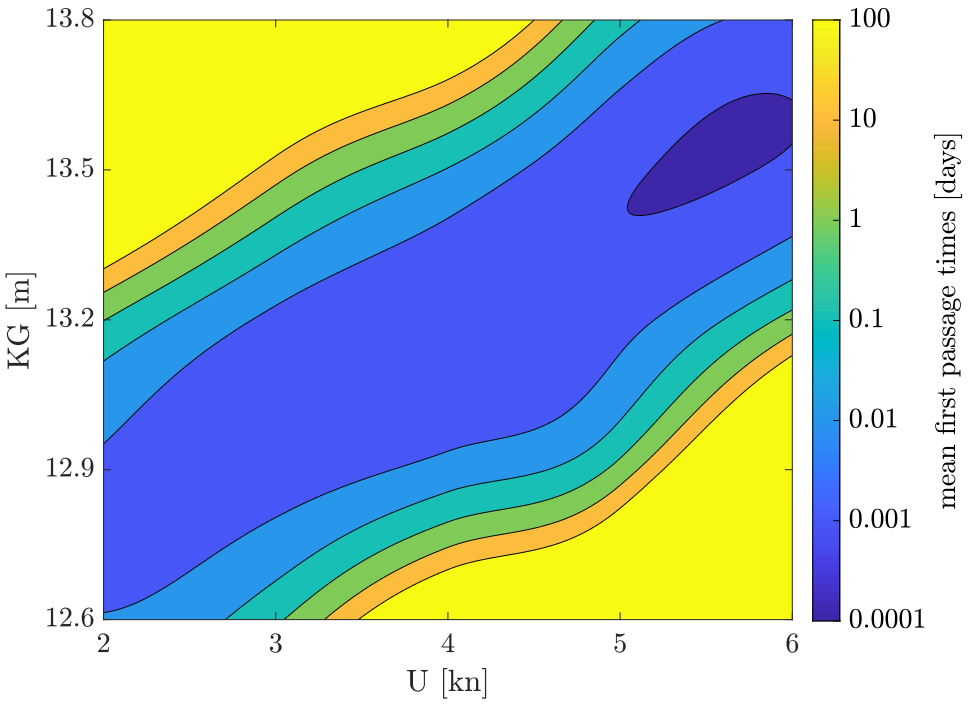

Figure 11: Mean first-passage times of roll amplitude $\varphi_c = 30°$ with respect to distance KG and ship speed U for the case of wave encounter angle $\chi_0 = 5°$, JONSWAP sea state with mean wave period $T_1 = 11.5$ s, and significant wave height $H_s = 3$ m

Moreover, the Jacobian elliptic functions $\mathrm{sn}(\cdot, k)$, $\mathrm{cn}(\cdot, k)$, $\mathrm{dn}(\cdot, k)$, and the complete elliptic integral of the first kind $K(k)$ are used, c.f. [51], where $k = b/a$ is the elliptic modulus. In addition the abbreviations

$$\begin{aligned} \mathrm{sn} &:= \mathrm{sn}(qt, k),\ \mathrm{cn} := \mathrm{cn}(qt, k),\ \mathrm{dn} := \mathrm{dn}(qt, k),\ u := qt \\ \mathrm{sn} &:= \mathrm{sn}(q(t+\tau), k),\ \mathrm{cn} := \mathrm{cn}(q(t+\tau), k),\ \mathrm{dn} := \mathrm{dn}(q(t+\tau), k), \end{aligned} \tag{A.4}$$

are introduced.

It is also possible to determine the drift and diffusion of the roll energy for the quintic case of the GZ curve in Eq. (26) with $N_\varphi = 5$, as derived in [37]. The results are stated in the following. First, the energy H^c corresponding to the energy when the oscillation reaches the angle of vanishing stability φ_c is introduced

$$H^c = \frac{1}{3}\alpha_1 b_c^2 + \frac{1}{12}\alpha_3 b_c^4, \tag{A.5}$$

where

$$b_c = \sqrt{\frac{\alpha_3 + \sqrt{\alpha_3^2 + 4\alpha_1\alpha_5}}{2\alpha_5}}. \tag{A.6}$$

Moreover the functions

$$U_5(x) := \alpha_1 \frac{x^2}{2} + \alpha_3 \frac{x^4}{4} - \alpha_5 \frac{x^6}{6},$$

$$Q_5(x, H) := y^2 = 2H - 2U_6(x, H), \tag{A.7}$$

and

$$G_5(x, H) := -\beta_1 - \beta_2 \sqrt{Q_5(x(t), H)} - \beta_3 Q_5(x(t), H) \tag{A.8}$$

are introduced. Then, for fixed $0 \leq H < H^c$, the drift and diffusion for the case with a quintic GZ curve with $N_\varphi = 5$ can be stated as

$$\begin{aligned} m(H) =& \frac{2}{Tq} \int_{-\infty}^{0} \Big\{ R_{\xi_1\xi_1}(\tau)\nu_1^2 \int_{-K(k)}^{K(k)} \frac{\mathrm{cn}_{t+\tau}\mathrm{dn}_{t+\tau}\,(c - d\mathrm{sn}^2)^{3/2}}{\mathrm{cn}\,\mathrm{dn}\,(c - d\mathrm{sn}_{t+\tau}{}^2)^{3/2}} \mathrm{d}u \\ &+ R_{\xi_2\xi_2}(\tau)\nu_2^2 \int_{-K(k)}^{K(k)} \mathrm{sn}\,\mathrm{sn}_{t+\tau} \frac{\mathrm{cn}_{t+\tau}\mathrm{dn}_{t+\tau}\,(c - d\mathrm{sn}^2)}{\mathrm{cn}\,\mathrm{dn}\,(c - d\mathrm{sn}_{t+\tau}{}^2)^2} \mathrm{d}u \Big\}\, \mathrm{d}\tau \\ &+ \frac{1}{T} \int_0^T Q_5(x(t), H) G_5(x(t), H) \mathrm{d}t, \end{aligned} \tag{A.9}$$

$$\begin{aligned} \sigma^2(H) =& \frac{4c^2 q}{T} \int_{-\infty}^{\infty} \Big\{ R_{\xi_1\xi_1}(\tau)\nu_1^2 \int_0^{K(k)} \frac{\mathrm{cn}\,\mathrm{dn}\,\mathrm{cn}_{t+\tau}\,\mathrm{dn}_{t+\tau}}{(c - d\mathrm{sn}^2)^{3/2}\,(c - d\mathrm{sn}_{t+\tau}{}^2)^{3/2}} \mathrm{d}u \\ &+ R_{\xi_2\xi_2}(\tau)\nu_2^2 \int_0^{K(k)} \frac{\mathrm{sn}\,\mathrm{sn}_{t+\tau}\mathrm{cn}\,\mathrm{dn}\,\mathrm{cn}_{t+\tau}\,\mathrm{dn}_{t+\tau}}{(c - d\mathrm{sn}^2)^2\,(c - d\mathrm{sn}_{t+\tau}{}^2)^2}\, \mathrm{d}u \Big\}\, \mathrm{d}\tau. \end{aligned} \tag{A.10}$$

The coefficients used in these expressions are given by

$$c = \frac{6\,Hw - \alpha_1 + \sqrt{-12\,H^2w^2 + 4\,Hw\alpha_1 + {\alpha_1}^2 + 4\,H\alpha_3}}{4H}, \tag{A.11}$$

$$d = c - w, \qquad q = \sqrt{2cH}. \tag{A.12}$$

Here, w is the root of the function

$$W(z) = -\frac{1}{3}\,\alpha_5 + \frac{1}{2}\,\alpha_3 z + \alpha_1 z^2 - 2\,Hz^3, \tag{A.13}$$

which is given by

$$w = \frac{v}{12H} + \frac{3\,\alpha_3 H + {\alpha_1}^2}{3v} + \frac{\alpha_1}{6H}, \tag{A.14}$$

where

$$v = \Big(36\,\alpha_3\alpha_1 H - 144\,\alpha_5 H^2 + 8\,{\alpha_1}^3 + 12\,H\,\sqrt{-12\,{\alpha_3}^3 H - 3\,{\alpha_3}^2{\alpha_1}^2 - 72\,\alpha_3\alpha_1 H\alpha_5 + 144\,{\alpha_5}^2 H^2 - 16\,\alpha_5{\alpha_1}^3}\Big)^{\frac{1}{3}}. \tag{A.15}$$

The elliptic modulus k of the Jacobi elliptic functions is obtained as

$$k^2 = 1 + 4\,\frac{(4\,\alpha_1 w - 12\,H w^2 + \alpha_3)\,H}{\left(6\,Hw - \alpha_1 + \sqrt{-12\,H^2 w^2 + 4\,Hw\alpha_1 + {\alpha_1}^2 + 4\,H\alpha_3}\right)^2}. \tag{A.16}$$

References

[1] L. Dostal, E. Kreuzer, Probabilistic approach to large amplitude ship rolling in random seas, Proceedings of the Institution of Mechanical Engineers, Part C: Journal of Mechanical Engineering Science 225 (2011) 2464–2476.

[2] O. Grim, Rollschwingungen, Stabilität und Sicherheit im Seegang, Schiffstechnik 1 (1952) 10–21.

[3] V. L. Belenky, C. C. Bassler, Procedures for early-stage naval ship design evaluation of dynamic stability: Influence of the wave crest, Naval Engineers Journal 122 (2010) 93–106.

[4] S. Krueger, F. Kluwe, Development of dynamic stability criteria from direct seakeeping simulations, in: Proceedings of 9th International Marine Design Conference. Ann Arbor, Michigan, Citeseer, pp. 16–19.

[5] L. Dostal, E. Kreuzer, N. Sri Namachchivaya, Non-standard stochastic averaging of large amplitude ship rolling in random seas, Proceedings of the Royal Society A: Mathematical, Physical and Engineering Sciences 468 (2012) 4146–4173.

[6] O. Grim, Beitrag zu dem Problem der Sicherheit des Schiffes im Seegang, Schiff und Hafen 6 (1961) 490–497.

[7] G. Bulian, On an improved Grim effective wave, Ocean Engineering 35 (2008) 1811–1825.

[8] N. Umeda, Y. Yamakoshi, Probability of ship capsizing due to pure loss of stability in quartering seas, Naval architecture and ocean engineering 30 (1992) 73–85.

[9] J. Hua, W.-H. Wang, J.-R. Chang, A representation of gm-variation in waves by the volterra system, Journal of marine science and technology 7 (2009) 4.

[10] A. S. Somayajula, J. Falzarano, A comparative assessment of simplified models for simulating parametric roll, Journal of Offshore Mechanics and Arctic Engineering 139 (2017).

[11] W. Blocki, Ship safety in connection with parametric resonance of the roll, Int. Shipbuilding Progr. 27 (1980) 36–53.

[12] N. Themelis, K. J. Spyrou, Probabilistic assessment of ship stability based on the concept of critical wave groups (2008).

[13] A. Maki, N. Umeda, S. Shiotani, E. Kobayashi, Parametric rolling prediction in irregular seas using combination of deterministic ship dynamics and probabilistic wave theory, Journal of marine science and technology 16 (2011) 294–310.

[14] J. B. Roberts, Effect of parametric excitation on ship rolling motion in random waves, J Ship Res 26 (1982) 246–253.

[15] R. L. Stratonovich, Topics in the Theory of Random Noise Volume I, Gordon and Breach, New York, 1963.

[16] R. Z. Khasminskii, A limit theorem for the solution of differential equations with random right-hand sides, Theory Probab Appl 11 (1966) 390–405.

[17] J. B. Roberts, M. Vasta, Response of non-linear oscillators to non-white random excitation using an energy based method, in: S. Narayanan, R. Iyengar (Eds.), Proc. IUTAM Symp. on Nonlinearity and Stochastic Structural Dynamics, Chennai, India.

[18] J. B. Roberts, M. Vasta, Markov modelling and stochastic identification for nonlinear ship rolling in random waves, Phil Trans R Soc Lond A 358 (2000) 1917–1941.

[19] R. Z. Khasminskii, On the principles of averaging for Itô stochastic differential equations, Kybernetica 4 (1968) 260–279.

[20] N. K. Moshchuk, R. A. Ibrahim, R. Z. Khasminskii, P. L. Chow, Asymptotic expansion of ship capsizing in random sea waves – I. First-order approximation, Int J Nonlinear Mech 30 (1995) 727–740.

[21] N. Moshchuk, R. Ibrahim, R. Khasminskii, P. Chow, Ship capsizing in random sea waves and the mathentical pendulum, in: IUTAM Symposium on Advances in Nonlinear Stochastic Mechanics, Springer, pp. 299–309.

[22] L. Pontryagin, A. Andronov, A. Vitt, On statistical consideration of dynamic systems, J. Exper. Theor. Phys 3 (1933) 165–180.

[23] L. Dostal, N. S. Namachchivaya, First passage time of nonlinear diffusion processes with singular boundary behavior, Journal of Sound and Vibration 476 (2020) 115284.

[24] Z. Ren, W. Xu, D. Wang, Dynamic and first passage analysis of ship roll motion with inelastic impacts via path integration method, Nonlinear Dynamics 97 (2019) 391–402.

[25] D. S. A. Hughes, Directional wave spectra using cosine-squared and cosine 2s spreading functions, Coastal Engineering Technical Note. Coastal Engineering Research Center, Coastal and hydraulics Laboratary (1985).

[26] S. Corbella, D. D. Stretch, Directional wave spectra on the east coast of south africa, Journal of the South African Institution of Civil Engineering= Joernaal van die Suid-Afrikaanse Instituut van Siviele Ingenieurswese 56 (2014) 53–64.

[27] H. Mitsuyasu, F. Tasai, T. Suhara, S. Mizuno, M. Okhuso, T. Honda, K. Rikiishi, Observation of the directional spectrum of ocean waves using a cloverleaf buoy, J. Physical Oceanogr 5 (1975) 750–760.

[28] M. Shinozuka, Simulation of multivariate and multidimensional random processes, The Journal of the Acoustical Society of America 49 (1971) 357–368.

[29] G. Clauss, E. Lehmann, C. Östergaard, Offshore Structures: Volume II Strength and Safety for Structural Design, Springer Science & Business Media, 2012.

[30] R. Beck, W. Cummins, J. Dalzell, P. Mandel, W. Webster, Principles of naval architecture, volume 3, motions in waves and controllability, The Society of Naval Architects and Marine Engineers, Jersey City (1989) 1–188.

[31] R. Bhattacharyya, Dynamics of marine vehicles, John Wiley & Sons Incorporated, 1978.

[32] G. Lindgren, I. Rychlik, M. Prevosto, Stochastic doppler shift and encountered wave period distributions in gaussian waves, Ocean Engineering 26 (1999) 507–518.

[33] S. Gaglione, S. Pennino, V. Piscopo, A. Scamardella, Absolute sea spectrum resampling from encounter wave time history, Proceedings of the IMEKO TC 19 (2019).

[34] G. Clauss, E. Lehmann, C. Östergaard, Offshore structures: volume I: conceptual design and hydromechanics, Springer, 2014.

[35] L. Dostal, E. Kreuzer, Assessment of extreme rolling of ships in random seas, in: Proc. of the ASME 2014 33rd International Conference on Ocean, Offshore and Arctic Engineering, San Francisco, USA.

[36] S. N. Blagoveshchensky, Theory of Ship Motions, Dover Publications, New York, 1962.

[37] L. Dostal, E. Kreuzer, Analytical and semi-analytical solutions of some fundamental nonlinear stochastic differential equations, Proc. IUTAM 19 (2016) 178–186.

[38] L. Dostal, K. Korner, E. Kreuzer, D. Yurchenko, Pendulum energy converter excited by random loads, Z. Angew. Math. Mech. 98 (2018) 349–366.

[39] N. Sri Namachchivaya, Stochastic bifurcation, Applied Mathematics and Computation 39 (1990) 37–95.

[40] J. Roberts, P. Spanos, Stochastic averaging: an approximate method of solving random vibration problems, International Journal of Non-Linear Mechanics 21 (1986) 111–134.

[41] N. Sri Namachchivaya, R. B. Sowers, L. Vedula, Non-standard reduction of noisy Duffing-van der Pol equation, Dynamical Systems 16 (2001) 223–245.

[42] M. I. Freidlin, A. D. Wentzell, Diffusion processes on graphs and the averaging principle, The Annals of probability (1993) 2215–2245.

[43] M. I. Freidlin, A. D. Wentzell, Random perturbations of Hamiltonian systems, volume 523, American Mathematical Soc., 1994.

[44] Y. Liu, L. Liu, L. Dostal, J. Lu, The applicability of stochastic averaging method to solve the ship rolling response excited by narrow-band waves, Ocean Engineering 251 (2022) 111109.

[45] J. B. Roberts, The energy envelope of a randomly excited non-linear oscillator, Journal of Sound and Vibration 60 (1978) 177–185.

[46] J. B. Roberts, A stochastic theory for nonlinear ship rolling in irregular seas, J Ship Res 26 (1982) 229–245.

[47] J. R. Red-Horse, P. D. Spanos, A generalization to stochastic averaging in random vibration, Int. J. Non-Linear Mechanics 27 (1992) 85–101.

[48] S. Karlin, M. H. Taylor, A Second Course in Stochastic Processes, Academic Press, New York, 1981.

[49] H. Krüger, S.and Hatecke, H. Billerbeck, A. Bruns, F. Kluwe, Investigation of the 2nd generation of intact stability criteria for ships vulnerable to parametric rolling in following seas, in: 32nd International Conference on Offshore Mechanics and Arctic Engineering, Nantes, France.

[50] P. Blume, Experimentelle Bestimmung von Koeffizienten der wirksamen Rolldämpfung und ihre Anwendung zur Abschätzung extremer Rollwinkel, Schiffstechnik 26 (1979) 3–23.

[51] P. F. Byrd, M. D. Friedman, Handbook of elliptic integrals for engineers and scientists, B. G. Teubner, Berlin, 1954.